

Optimization of iterative reconstruction parameters with attenuation correction, scatter correction and resolution recovery in myocardial perfusion SPECT/CT

Koichi Okuda · Kenichi Nakajima · Masato Yamada · Hiroshi Wakabayashi · Hajime Ichikawa · Hiroyuki Arai · Shinro Matsuo · Junichi Taki · Mitsumasa Hashimoto · Seigo Kinuya

Received: 24 July 2013 / Accepted: 19 October 2013 / Published online: 9 November 2013
© The Japanese Society of Nuclear Medicine 2013

Abstract

Objective The aim of this study was to characterize the optimal reconstruction parameters for ordered-subset expectation maximization (OSEM) with attenuation correction, scatter correction, and depth-dependent resolution recovery (OSEM_{ACSCRR}). We assessed the optimal parameters for OSEM_{ACSCRR} in an anthropomorphic torso phantom study, and evaluated the validity of the reconstruction parameters in the groups of normal volunteers and patients with abnormal perfusion.

Methods Images of the anthropomorphic torso phantom, 9 normal volunteers and 7 patients undergoing myocardial perfusion SPECT were acquired with a SPECT/CT scanner. SPECT data comprised a 64 × 64 matrix with an acquisition pixel size of 6.6 mm. A normalized mean

square error (NMSE) of the phantom image was calculated to determine both optimal OSEM update and a full width at half maximum (FWHM) of Gaussian filter. We validated the myocardial count, contrast and noise characteristic for clinical subjects derived from OSEM_{ACSCRR} processing. OSEM with depth-dependent resolution recovery (OSEM_{RR}) and filtered back projection (FBP) were simultaneously performed to compare OSEM_{ACSCRR}.

Results The combination of OSEM_{ACSCRR} with 90–120 OSEM updates and Gaussian filter with 13.2–14.85 mm FWHM yielded low NMSE value in the phantom study. When we used OSEM_{ACSCRR} with 120 updates and Gaussian filter with 13.2 mm FWHM in the normal volunteers, myocardial contrast showed significantly higher value than that derived from 120 updates and 14.85 mm FWHM. OSEM_{ACSCRR} with the combination of 90–120 OSEM updates and 14.85 mm FWHM produced lowest % root mean square (RMS) noise. Regarding the defect contrast of patients with abnormal perfusion, OSEM_{ACSCRR} with the combination of 90–120 OSEM updates and 13.2 mm FWHM produced significantly higher value than that derived from 90–120 OSEM updates and 14.85 mm FWHM. OSEM_{ACSCRR} was superior to FBP for the % RMS noise (8.52 ± 1.08 vs. 9.55 ± 1.71 , $p = 0.02$) and defect contrast (0.368 ± 0.061 vs. 0.327 ± 0.052 , $p = 0.01$), respectively.

Conclusions Clinically optimized the number of OSEM updates and FWHM of Gaussian filter were (1) 120 updates and 13.2 mm, and (2) 90–120 updates and 14.85 mm on the OSEM_{ACSCRR} processing, respectively. Further assessment may be required to determine the optimal iterative reconstruction parameters in a larger patient population.

K. Okuda (✉) · M. Hashimoto
Department of Physics, Kanazawa Medical University, 1-1 Daigaku, Uchinada, Kahoku, Ishikawa 920-0293, Japan
e-mail: okuda@kanazawa-med.ac.jp

K. Nakajima (✉) · H. Wakabayashi · S. Matsuo · J. Taki · S. Kinuya
Department of Nuclear Medicine, Kanazawa University Hospital, 13-1 Takara-machi, Kanazawa 920-8641, Japan
e-mail: nakajima@med.kanazawa-u.ac.jp

M. Yamada
Kanazawa Advanced Medical Center, 13-1 Takara-machi, Kanazawa 920-8641, Japan

H. Ichikawa
Department of Radiology, Toyohashi Municipal Hospital, 50 Hachiken Nishi, Aotake, Toyohashi, Aichi 441-8570, Japan

H. Arai
Siemens Japan, 1-11-1 Osaki, Shinagawa-ku, Tokyo 141-8603, Japan

Keywords Myocardial perfusion SPECT · Ordered-subset expectation maximization · Attenuation

correction · Scatter correction · Depth-dependent resolution recovery

Introduction

Iterative reconstruction [1], such as ordered-subset expectation maximization (OSEM) [2], is an indispensable technology for the corrections of depth-dependent blurring, photon attenuation and scatter in the field of nuclear medicine. As for myocardial perfusion single-photon emission computed tomography (SPECT) imaging (MPI), iterative reconstruction improves the signal-to-noise ratio of myocardial perfusion counts and the myocardial uptake overlapped with the hepatic uptake. Attenuation correction (AC), scatter correction (SC), and resolution recovery (RR) algorithm can be incorporated into the iterative reconstruction processing, which is suggested for the cardiac SPECT in the European Association of Nuclear Medicine/European Society of Cardiology guidelines [3, 4].

The latest iterative reconstruction technologies [5, 6] are commercially available as Flash 3D (Siemens Medical Solutions, Erlangen, Germany) [7–9], Astonish (Philips Medical Systems, Milpitas, CA, USA) [10–12], Evolution for Cardiac (GE Healthcare, Waukesha, WI, USA) [13] and wide beam reconstruction (UltraSPECT, Haifa, Israel) [13, 14]. Since noise reduction algorithm is incorporated into the latest iterative reconstruction processing as well as AC, SC and RR, half-time cardiac SPECT imaging became feasible [11, 13–16]. Consequently, the image quality for the half-time SPECT imaging is equivalent to that for the conventional full-time SPECT imaging in clinical studies [11, 13, 16].

However, optimal reconstruction parameters have not been clearly described in the latest cardiac OSEM processing with AC, SC and RR algorithm (OSEM_{ACSCRR}). In addition, an optimal cutoff value for filter processing also has not been characterized. The goal of this study was to determine the optimal OSEM reconstruction parameters on Flash 3D processing. We initially determined the optimal parameters in an anthropomorphic torso phantom study. Consequently, we applied the optimized OSEM parameters to a clinical MPI study, and evaluated myocardial count, contrast and noise characteristic in the groups of normal volunteers and patients with abnormal perfusion.

Materials and methods

Anthropomorphic torso phantom

We utilized an anthropomorphic torso phantom configured with the cardiac, pulmonary and hepatic components

(Kyoto Kagaku, Kyoto, Japan). The left ventricular (LV) myocardium and liver were filled with 199 and 24 MBq of Tc-99m pertechnetate, respectively. The left and right ventricular cavities were filled with water. Four plastic circular defects with 20 mm diameter were placed in the mid-anterior, lateral, inferior, and septal walls.

Study population

The population included 9 normal volunteers (6 males, mean age 31 ± 10) and 7 patients with abnormal perfusion (4 males, mean age 80 ± 6). There was no statistically difference between the body heights of the two groups as well as body weights (158 ± 11 vs. 165 ± 7 cm, 54 ± 11 vs. 60 ± 10 kg, respectively). The averages of ejection fraction (EF), end-systolic volume (ESV) and end-diastolic volume (EDV) were 65 ± 6 %, 29 ± 15 ml and 78 ± 25 ml for the normal volunteers, and 55 ± 13 %, 53 ± 50 ml and 108 ± 77 ml for the patients with abnormal perfusion, respectively. Averaged summed rest score (SRS) was 16.7 ± 7.1 for the patients with abnormal perfusion. The institutional ethical committee approved the normal volunteer study, and all volunteers gave informed consent. We retrospectively enrolled the patients with abnormal perfusion, who underwent rest gated MPI. All phantom and clinical researches were performed at Kanazawa University Hospital.

Image acquisition and data processing

Single-photon emission computed tomography acquisition was performed with a dual-head gamma camera (Symbia T6 hybrid SPECT/CT scanner, Siemens Japan, Tokyo, Japan) equipped with a low-energy high-resolution collimator. A photopeak window of ^{99m}Tc was set as a 15 % energy window centered at 140 keV, and a low sub-window for SC was set as a 7 % of photopeak window (120–129 keV). The acquisition pixel size was a 6.6 mm for a 64×64 matrix. In the phantom study, we acquired two axial images, which were reconstructed by 60 projection data, to calculate the normalized mean square error (NMSE) [17, 18]. In the clinical study, we performed rest gated- ^{99m}Tc -sestamibi (MIBI) MPI with 16 frames per cardiac cycle on the hybrid SPECT/CT scanner. MPI was performed with the 360° circular acquisition with 60 projections at 40 min after injection of ^{99m}Tc MIBI of 300–370 MBq. An acquisition time was set as 35 s per projection. We acquired a low-dose computed tomography (CT) image for AC using a 6-detector row CT on the SPECT/CT scanner. Tube voltage and effective mAs for AC CT were 130 kV and 20 mAs, respectively. The axial image was reconstructed with a thickness of 5.0 mm.

Data analysis

We used three reconstruction processings: OSEM_{ACSCRR}, OSEM with RR (OSEM_{RR}) and filtered back projection (FBP) in the phantom and clinical studies. AC SC and RR algorithm was not incorporated into the conventional FBP processing. When the number of subsets was constantly set as 15, the number of iterations was set from 1 to 30 (the range of OSEM updates, 15–450). We utilized Gaussian post-filter for both OSEM_{ACSCRR} and OSEM_{RR}, and Butterworth filter for FBP. The full width at half maximum (FWHM) of Gaussian filter was set from 6.6 to 14.85 mm. The cutoff frequency for Butterworth filter was set as 0.68 Nyquist. All the OSEM_{ACSCRR}, OSEM_{RR} and FBP were processed using the e.soft version 8.1 (Siemens Japan, Tokyo, Japan).

When we calculated NMSE value for the phantom imaging, the equation of NMSE calculation was as follows:

$$\text{NMSE} = \frac{\sum_{i=1}^x \sum_{j=1}^y \sum_{k=1}^z ((\text{Reference}(i, j, k) - \text{Test}(i, j, k))^2)}{\sum_{i=1}^x \sum_{j=1}^y \sum_{k=1}^z (\text{Reference}(i, j, k))^2},$$

where the Reference(*i, j, k*) represented a predicted pixel value on a reference standard image. The Test(*i, j, k*) represented an actual pixel value on a test image. An acquisition time for the reference standard imaging was set at ten times as much as that for the test imaging. Summed acquisition counts for the reference and test images were 18.1 and 1.8 million, respectively. The projection data for the reference and test imaging were reconstructed using OSEM_{ACSCRR} with the combinations of OSEM updates (15–450) and FWHM of Gaussian filter (6.6–14.85 mm).

Averaged LV count was calculated using the circumferential profile analysis in the apical, mid and basal short-axis slices. % root mean square (RMS) noise for the LV counts was defined as the equation of (standard deviation/mean) × 100. Myocardial contrast was also defined as the equation of (maximum LV count – background)/(maximum LV count + background). An averaged background count was calculated using square region of interest (3 × 3 pixels) at the center of the ventricular cavity on the mid and basal short-axis slices. In the clinical assessment of patients with abnormal perfusion, we defined the region of perfusion defect as a background count, and calculated the defect contrast.

SRS, EF, ESV and EDV were automatically calculated with quantitative perfusion SPECT (QPS) and quantitative gated SPECT (QGS) version 2008.1 (Cedars-Sinai Medical Center, Los Angeles, CA, USA). FBP processing was used to reconstruct the image for the calculation of EF and left

ventricular volume. SRS was calculated using a 17-segment model for LV segmentation. When we calculated SRS in the patients with abnormal perfusion, sex-specific, attenuation-corrected normal databases were utilized.

Statistical analysis

All continuous values were expressed as mean ± standard deviation. A paired *t* test was used to analyze the differences in paired continuous data. A one-way repeated measure analysis of variance was used to analyze the parametric data, and the pairwise comparison was performed using the Bonferroni correction for *p* values. The Friedman test was also used to analyze the non-parametric data. All statistical tests were two-tailed, and a *p* value of less than 0.05 was considered significant. These analyses were performed by using MedCalc software version 11.2.1.0 (Mariakerte, Belgium).

Results

Figure 1 shows the vertical long-axis and horizontal long-axis and short-axis displays of the reconstructed phantom image derived from OSEM_{ACSCRR}, OSEM_{RR} and FBP. OSEM_{ACSCRR} showed better uniformity of phantom activity concentration and myocardial delineation in comparison with OSEM_{RR} and FBP. Figure 2 shows NMSE value for the anthropomorphic phantom image derived from OSEM_{ACSCRR}. When we used Gaussian filter with 13.20 mm FWHM, NMSE value reached a plateau at 90 OSEM updates, and lower NMSE value was observed at 120 OSEM updates. In addition, there was no significant difference between NMSE values derived from Gaussian filters with 13.2 and 14.85 mm FWHMs. Consequently we focused on myocardial contrast, % RMS noise and defect contrast derived from OSEM_{ACSCRR} with 90 and 120 updates in the following clinical study, and also focused on those from Gaussian filter with 13.2 and 14.85 mm FWHMs.

Figure 3a shows the relationship between OSEM update and the average of normalized myocardial count in the normal volunteer group. When we used Gaussian filters with 13.2 and 14.85 mm FWHMs, myocardial counts reached plateaus at 120 OSEM updates. Figure 3b shows the relationship between OSEM update and contrast for normal myocardial uptake. There was significant difference between the contrasts derived from Gaussian filters with 13.2 and 14.85 mm FWHMs. There was also significant difference between the contrasts derived from 90 and 120 OSEM updates. OSEM_{ACSCRR} with 120 OSEM updates and Gaussian filter with 13.2 mm FWHM showed the highest contrast in the combination of 90–120 OSEM

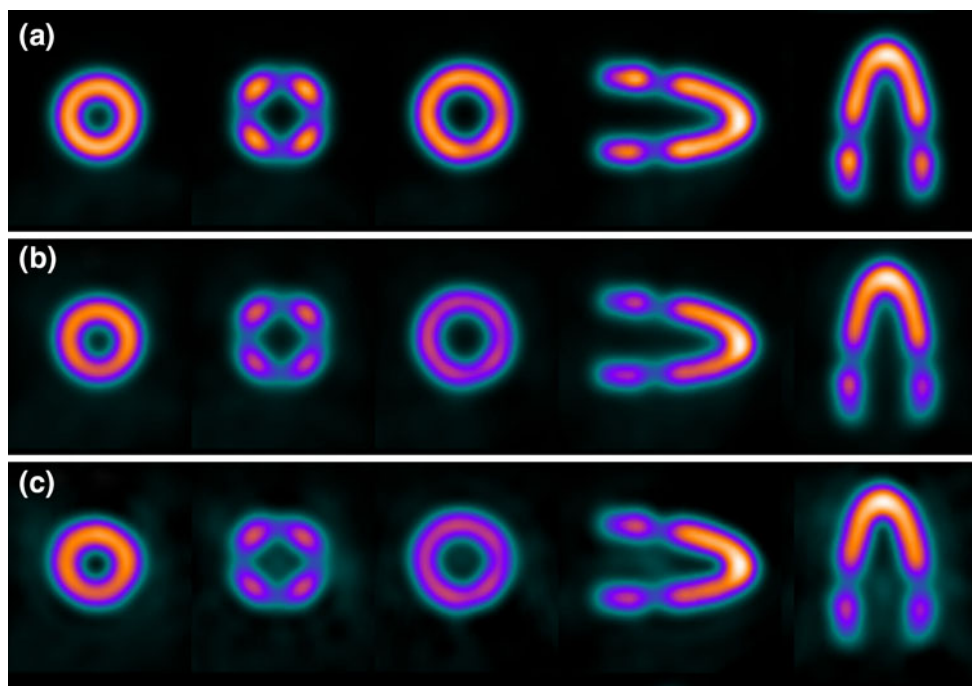


Fig. 1 Vertical long-axis, horizontal long-axis and (apical, mid and basal) short-axis displays of anthropomorphic phantom derived from OSEM_{ACSCRR} (a), OSEM_{RR} (b) and FBP (c). 120 OSEM updates and

Gaussian filter with 13.2 mm FWHM were used for OSEM_{ACSCRR} and OSEM_{RR}

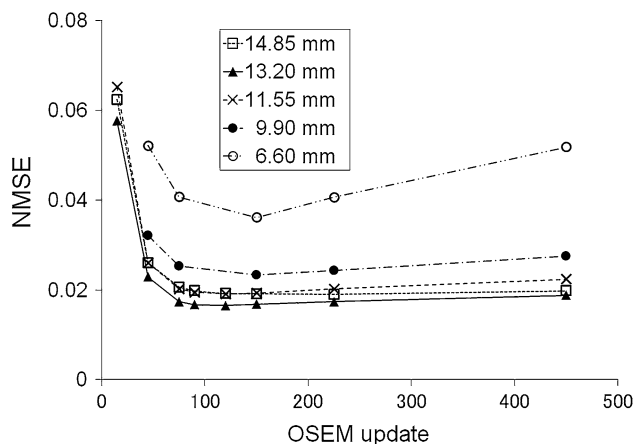


Fig. 2 NMSE value derived from OSEM_{ACSCRR} on the anthropomorphic torso phantom study. The FWHM of Gaussian filter was set from 6.60 to 14.85 mm

updates and Gaussian filter with 13.2–14.85 mm FWHM. Figure 3c shows the relationship between OSEM update and % RMS noise. Although significant difference was observed in the % RMS noises derived from Gaussian filters with 13.2 and 14.85 mm FWHMs, no significant difference was observed between 90 and 120 OSEM updates. Figure 4 shows the relationship between OSEM update and defect contrast. When we used Gaussian filters with 13.2 and 14.85 mm FWHMs, defect contrasts reached plateaus at 90 OSEM updates. There was significant difference

between the defect contrasts derived from the Gaussian filters with 13.2 and 14.85 mm FWHMs.

Figure 5 shows a flow chart for the optimization process of iterative reconstruction parameters. We experimentally characterized the optimized OSEM update and FWHM of Gaussian filter as 90–120 and 13.2–14.85 mm in the anthropomorphic torso phantom study, respectively. Consequently, after we evaluated the contrast for normal uptake, % RMS noise and defect contrast in the clinical MPI study, the optimized OSEM update and FWHM of Gaussian filter were characterized as both (1) 90–120 OSEM updates and Gaussian filter with 14.85 mm FWHM and (2) 120 OSEM updates and Gaussian filter with 13.2 mm FWHM.

Table 1 shows the comparison between OSEM_{ACSCRR} and FBP in the results of contrast for normal myocardial uptake, % RMS noise and defect contrast. Contrast for normal myocardial uptake derived from OSEM_{ACSCRR} was equivalent to that from FBP. % RMS noises derived from OSEM_{ACSCRR} with 90–120 updates and Gaussian filter with 14.85 mm FWHM were better than that from FBP (8.52 ± 1.08 and 8.45 ± 0.91 vs. 9.55 ± 1.71 , $p = 0.02$, respectively). Defect contrasts derived from OSEM_{ACSCRR} with 90–120 updates and Gaussian filter with 13.2 mm FWHM showed significantly higher values than that from FBP (0.368 ± 0.061 and 0.371 ± 0.061 vs. 0.327 ± 0.052 , $p \leq 0.01$).

Fig. 3 Relationships between OSEM update and normalized count (a), contrast (b) and noise characteristic (%RMS noise) (c) of the left ventricular uptake derived from OSEM_{ACSCRR} in the normal volunteer group.

Horizontal dotted line shows the contrast and % RMS noise derived from FBP in b and c

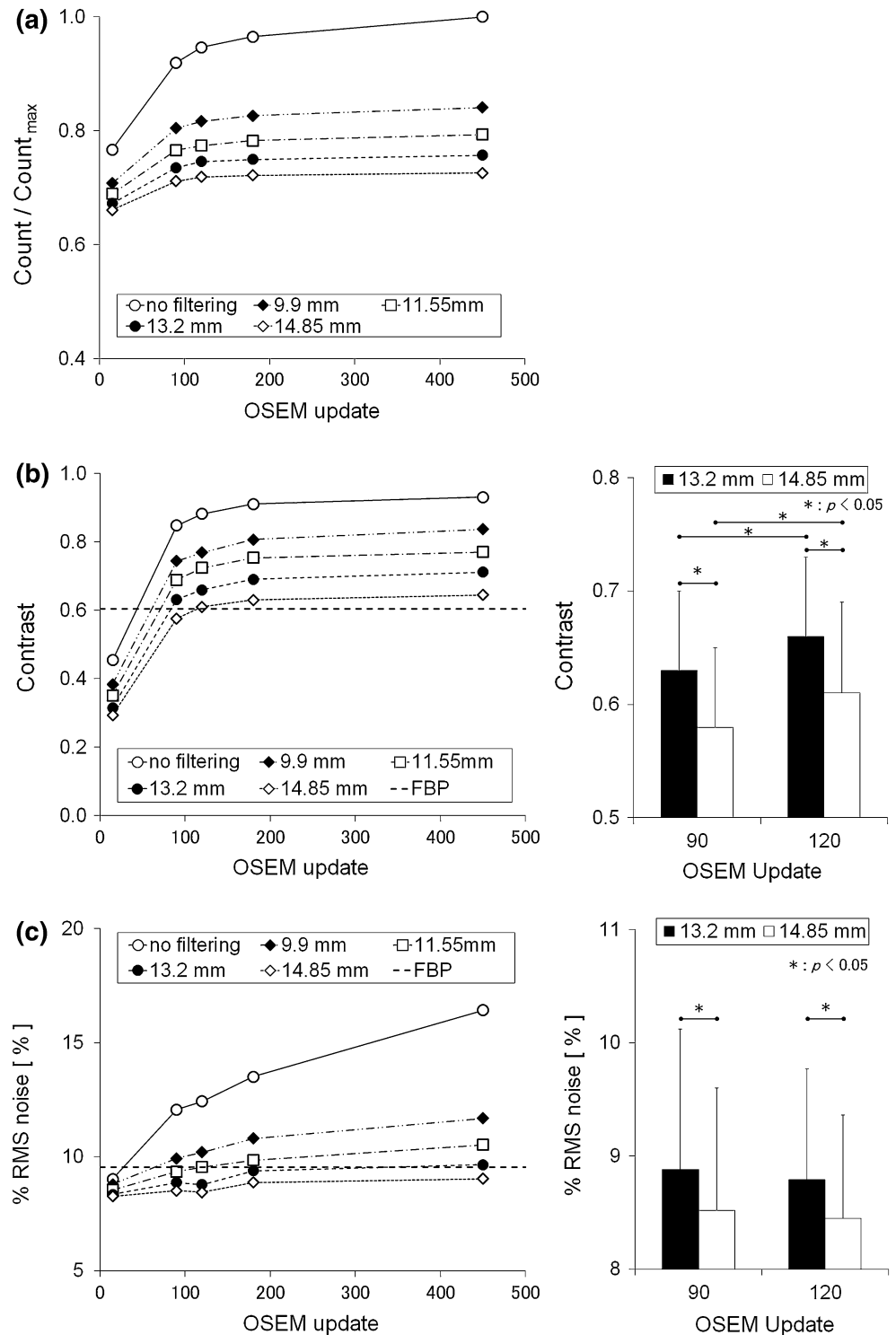


Figure 6 shows the vertical long-axis, horizontal long-axis and (apical, mid and basal) short-axis displays of the normal volunteer and patient with abnormal perfusion derived from OSEM_{ACSCRR}, OSEM_{RR} and FBP. When we used OSEM_{ACSCRR} with the optimized reconstruction parameters, myocardial infarction was clearly delineated.

Discussion

We characterized the optimal iterative reconstruction parameters for OSEM_{ACSCRR} processing in the phantom and clinical studies. In the phantom study, OSEM_{ACSCRR} with 90–120 updates and Gaussian filter with

Fig. 4 Relationship between OSEM update and defect contrast for patients with abnormal perfusion. Horizontal dotted line shows the defect contrast derived from FBP

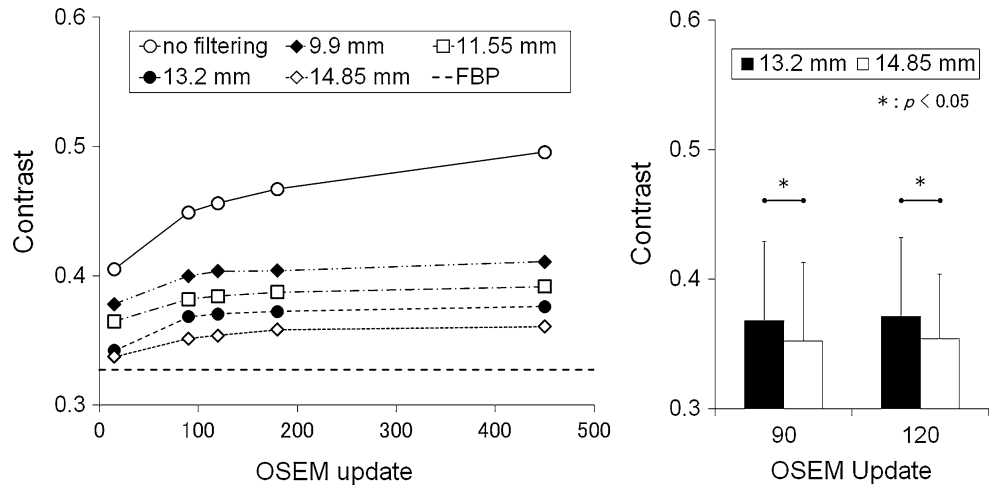


Fig. 5 Flow chart for the optimization process of iterative reconstruction parameters

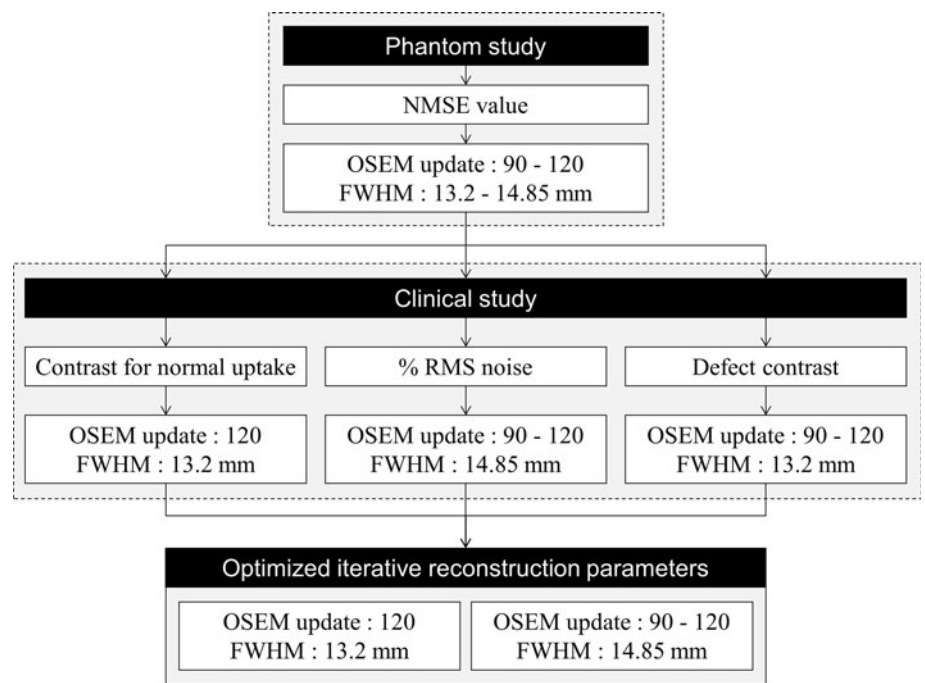


Table 1 Results of contrast between normal myocardial uptake and background, % RMS noise and defect contrast derived from OSEM_{ACSCRC} and FBP

OSEM update	FWHM of Gaussian filter		FWHM of Gaussian filter		FBP
	13.2 mm	p value (vs. FBP)	14.85 mm	p value (vs. FBP)	
Contrast between normal myocardial uptake and background					
90	0.63 ± 0.07	n.s.	0.58 ± 0.07	n.s.	0.60 ± 0.10
120	0.66 ± 0.07	n.s.	0.61 ± 0.08	n.s.	
% RMS noise					
90	8.88 ± 1.24	n.s.	8.52 ± 1.08	0.02	9.55 ± 1.71
120	8.79 ± 0.98	n.s.	8.45 ± 0.91	0.02	
Defect contrast					
90	0.368 ± 0.061	0.01	0.352 ± 0.061	n.s.	0.327 ± 0.052
120	0.371 ± 0.061	<0.01	0.354 ± 0.050	n.s.	

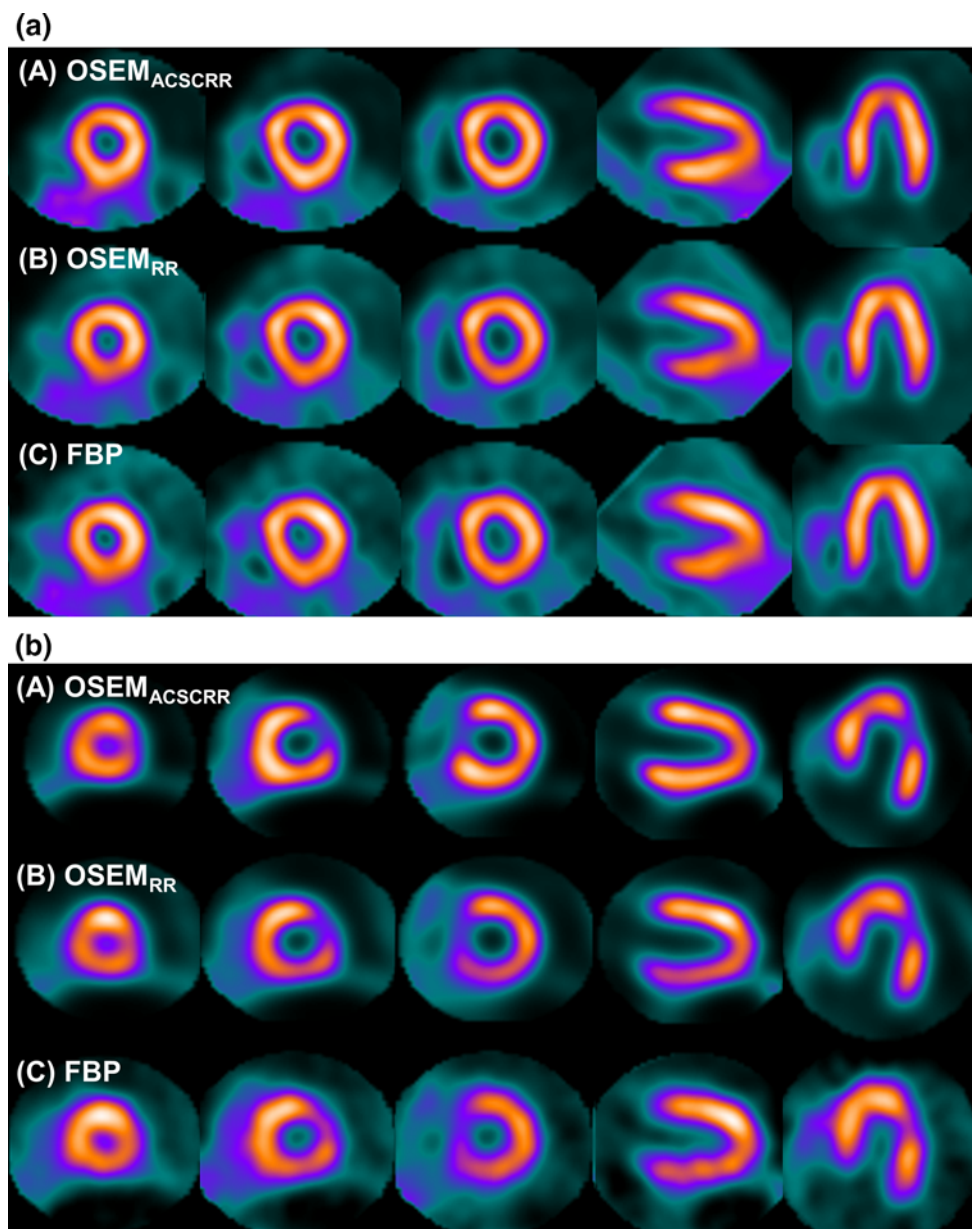


Fig. 6 Example of vertical long-axis, horizontal long-axis and (apical, mid and basal) short-axis displays of the normal volunteer (a) and patient with abnormal perfusion (b). 120 OSEM updates and Gaussian filter with 13.2 mm FWHM were used in the $OSEM_{ACSCRR}$ and $OSEM_{RR}$

13.2–14.85 mm FWHM produced low NMSE value. We determined that the clinically optimized iterative reconstruction parameters were both (1) 90 OSEM updates with 14.85 mm FWHM and (2) 90–120 OSEM updates with 13.2–14.85 mm FWHM in the groups of normal volunteers and patients with abnormal perfusion.

The optimizations for OSEM reconstruction parameters have been described in many studies. The number of updates for OSEM with no compensation was ranged from 8 to 50 in the bone, gallium and MPI studies [19–22]. As for $OSEM_{ACSCRR}$ processing in clinical MPI studies, 75 OSEM updates were used [23, 24]. Comparing the optimal

number of OSEM updates between $OSEM_{ACSCRR}$ and OSEM with no compensation, $OSEM_{ACSCRR}$ required more OSEM updates than OSEM with no compensation to reconstruct the projection data. However, Astonish technology required only 24 OSEM updates in clinical MPI study [12]. Moreover, when we used the wide beam reconstruction technology, suitable number of OSEM updates was automatically determined. We will need further investigation of the latest $OSEM_{ACSCRR}$ processing [18].

The combination of OSEM update and Gaussian filter significantly affected the perfusion count, contrast and

noise characteristic in the phantom and clinical studies. Moreover, there was a trade-off between the number of OSEM updates and the FWHM of Gaussian filter. For example, the delineation of normal myocardium derived from OSEM_{ACSCRR} with 90 updates and Gaussian filtering occasionally shows equivalent to that from OSEM_{ACSCRR} with 50 updates and no filtering. However, OSEM_{ACSCRR} with 50 updates is not enough to correct a depth-dependent blurring. Therefore, when the number of OSEM updates has been increased until the measured reconstruction data matches with the estimated reconstruction data, Gaussian filter should be applied to the reconstructed image to decrease the statistical noise.

Clinical implication of this study was that we experimentally determined that the optimized iterative reconstruction parameters were both 90 OSEM updates with 13.2 mm-FWHM Gaussian filter and 90–120 OSEM updates with 13.2–14.85 mm-FWHM Gaussian filter in the clinical MPI studies. In comparison with FBP processing, % RMS noise and defect delineation were significantly improved with OSEM_{ACSCRR} processing. Whereas, normal myocardial contrast derived from OSEM_{ACSCRR} was equivalent to that from FBP. In the diagnostic performances of clinical MPI using OSEM_{ACSCRR}, OSEM_{ACSCRR} was superior to FBP regarding the sensitivity (82.2 ± 2.7 vs. 65.9 ± 4.9 , $p < 0.001$) and specificity (82.6 ± 3.0 vs. 66.7 ± 4.5 , $p = 0.001$) for the detection of coronary artery disease (CAD) [24]. Pretorius also reported that OSEM_{ACSCRR} yielded significantly better detection of CAD than FBP [23].

Our study has several limitations. We did not describe the optimal number of subsets. In our preliminary study for the evaluation of subset, when we acquired 60 projection datasets using the NEMA IEC PET phantom, equivalent image quality was visually observed among the OSEM updates of 15 subsets \times 6 iterations, 10 subsets \times 9 iterations, 6 subsets \times 15 iterations, 5 subsets \times 18 iterations, and 3 subsets \times 30 iterations. In the low-count SPECT imaging, optimal number of OSEM updates may be modified. This is because reconstructed image quality is determined by the count statistics within the subset. We will need the further investigation for optimal OSEM reconstruction parameters in the low-count acquisition. Finally, we did not have enough normal volunteers and patients with abnormal perfusion to evaluate the myocardial count, contrast and noise characteristic. Further assessment may be needed to confirm this observation in a larger patient population.

Conclusion

We determined that the optimized OSEM update and FWHM of Gaussian filter were both (1) 90 updates and

13.2 mm and (2) 90–120 updates and 13.2–14.85 mm in the clinical MPI study, respectively. OSEM_{ACSCRR} processing was superior to FBP processing for the noise characteristic and defect delineation, and equivalent to FBP processing for the myocardial contrast. Further assessment may be needed to confirm the optimized reconstruction parameters in a larger patient population.

Acknowledgments We thank nuclear medicine technologists: Minoru Tobisaka, Prof. Masahisa Onoguchi, Shigeto Matsuyama, Hiroto Yoneyama, Masakazu Kobayashi, Hironori Kojima, Takahiro Konishi, Keita Sakuta, Haruka Koshida (Kanazawa University Hospital, Kanazawa, Japan) for their assistance. We also thank Carole Fujioka, DVM for the grammatical revision. This work was supported in part by JSPS KAKENHI Grant Number 22591320 and Grant for Promoted Research from Kanazawa Medical University (S2013-16).

Conflict of interest Authors declare no conflict of interest in this study.

References

1. Shepp LA, Vardi Y. Maximum likelihood reconstruction for emission tomography. *IEEE Trans Med Imaging*. 1982;1:113–22.
2. Hudson HM, Larkin RS. Accelerated image reconstruction using ordered subsets of projection data. *IEEE Trans Med Imaging*. 1994;13:601–9.
3. Hesse B, Tagil K, Cuocolo A, Anagnostopoulos C, Bardies M, Bax J, et al. EANM/ESC procedural guidelines for myocardial perfusion imaging in nuclear cardiology. *Eur J Nucl Med Mol Imaging*. 2005;32:855–97.
4. Hesse B, Lindhardt TB, Acampa W, Anagnostopoulos C, Ballinger J, Bax JJ, et al. EANM/ESC guidelines for radionuclide imaging of cardiac function. *Eur J Nucl Med Mol I*. 2008;35:851–85.
5. Slomka PJ, Patton JA, Berman DS, Germano G. Advances in technical aspects of myocardial perfusion SPECT imaging. *J Nucl Cardiol*. 2009;16:255–76.
6. Zaman MU, Hashmi I, Fatima N. Recent developments and future prospects of SPECT myocardial perfusion imaging. *Ann Nucl Med*. 2010;24:565–9.
7. Zeintl J, Vija AH, Yahil A, Hornegger J, Kuwert T. Quantitative accuracy of clinical ^{99m}Tc SPECT/CT using ordered-subset expectation maximization with 3-dimensional resolution recovery, attenuation, and scatter correction. *J Nucl Med*. 2010;51:921–8.
8. Ficarò EP, Kritzman JN, Corbett JR. Effect of reconstruction parameters and acquisition times on myocardial perfusion distribution in normals. *J Nucl Cardiol*. 2008;15:S20.
9. Ceriani L, Ruberto T, Delaloye AB, Prior JO, Giovannella L. Three-dimensional ordered-subset expectation maximization iterative protocol for evaluation of left ventricular volumes and function by quantitative gated SPECT: a dynamic phantom study. *J Nucl Med Technol*. 2010;38:18–23.
10. Bateman TM, Heller GV, McGhie AI, Courter SA, Golub RA, Case JA, et al. Multicenter investigation comparing a highly efficient half-time stress-only attenuation correction approach against standard rest-stress Tc-99m SPECT imaging. *J Nucl Cardiol*. 2009;16:726–35.
11. Venero CV, Heller GV, Bateman TM, McGhie AI, Ahlberg AW, Katten D, et al. A multicenter evaluation of a new post-

- processing method with depth-dependent collimator resolution applied to full-time and half-time acquisitions without and with simultaneously acquired attenuation correction. *J Nucl Cardiol.* 2009;16:714–25.
12. Tashiro K, Tomiguchi S, Shiraishi S, Yoshida M, Sakaguchi F, Yamashita Y. Clinical usefulness of a collimator distance dependent resolution recovery in myocardial perfusion SPECT: a clinical report from a single institute. *Ann Nucl Med.* 2011;25:133–7.
 13. DePuey EG, Bommireddipalli S, Clark J, Leykekhman A, Thompson LB, Friedman M. A comparison of the image quality of full-time myocardial perfusion SPECT vs wide beam reconstruction half-time and half-dose SPECT. *J Nucl Cardiol.* 2011;18:273–80.
 14. Borges-Neto S, Pagnanelli RA, Shaw LK, Honeycutt E, Shwartz SC, Adams GL, et al. Clinical results of a novel wide beam reconstruction method for shortening scan time of Tc-99m cardiac SPECT perfusion studies. *J Nucl Cardiol.* 2007;14:555–65.
 15. Valenta I, Treyer V, Husmann L, Gaemperli O, Schindler MJ, Herzog BA, et al. New reconstruction algorithm allows shortened acquisition time for myocardial perfusion SPECT. *Eur J Nucl Med Mol Imaging.* 2010;37:750–7.
 16. DePuey EG, Gadiraju R, Clark J, Thompson L, Anstett F, Shwartz SC. Ordered subset expectation maximization and wide beam reconstruction “half-time” gated myocardial perfusion SPECT functional imaging: a comparison to “full-time” filtered backprojection. *J Nucl Cardiol.* 2008;15:547–63.
 17. Penney BC, King MA, Schwinger RB, Baker SP, Stritzke P, Doherty PW. Constrained least-squares restoration of nuclear medicine images: selecting the coarseness function. *Med Phys.* 1987;14:849–58.
 18. Onishi H, Motomura N, Fujino K, Natsume T, Haramoto Y. Quantitative performance of advanced resolution recovery strategies on SPECT images: evaluation with use of digital phantom models. *Radiol Phys Technol.* 2013;6:42–53.
 19. Blocklet D, Seret A, Popa N, Schoutens A. Maximum-likelihood reconstruction with ordered subsets in bone SPECT. *J Nucl Med.* 1999;40:1978–84.
 20. Case JA, Licho R, King MA, Weaver JP. Bone SPECT of the spine: a comparison of attenuation correction techniques. *J Nucl Med.* 1999;40:604–13.
 21. Wells RG, King MA, Simkin PH, Judy PF, Brill AB, Gifford HC, et al. Comparing filtered backprojection and ordered-subsets expectation maximization for small-lesion detection and localization in 67 Ga SPECT. *J Nucl Med.* 2000;41:1391–9.
 22. Takahashi Y, Murase K, Higashino H, Sogabe I, Sakamoto K. Receiver operating characteristic (ROC) analysis of images reconstructed with iterative expectation maximization algorithms. *Ann Nucl Med.* 2001;15:521–5.
 23. Pretorius PH, King MA, Gifford HC, Dahlberg ST, Spencer F, Simon E, et al. Myocardial perfusion SPECT reconstruction: receiver operating characteristic comparison of CAD detection accuracy of filtered backprojection reconstruction with all of the clinical imaging information available to readers and solely stress slices iteratively reconstructed with combined compensation. *J Nucl Cardiol.* 2005;12:284–93.
 24. Narayanan MV, King MA, Pretorius PH, Dahlberg ST, Spencer F, Simon E, et al. Human-observer receiver-operating-characteristic evaluation of attenuation, scatter, and resolution compensation strategies for (99m)Tc myocardial perfusion imaging. *J Nucl Med.* 2003;44:1725–34.